

A four-node hybrid assumed-strain finite element for laminated composite plates

A. Cazzani¹, E. Garusi², A. Tralli³ and S.N. Atluri⁴

Summary

Fibre-reinforced plates and shells are finding an increasing interest in engineering applications. Consequently, efficient and robust computational tools are required for the analysis of such structural models. As a matter of fact, a large amount of laminate finite elements have been developed and incorporated in most commercial codes for structural analysis.

In this paper a new laminate hybrid assumed-strain plate element is derived within the framework of the First-order Shear Deformation Theory (i.e. assuming that particles of the plate originally lying along a straight line which is normal to the undeformed middle surface remain aligned along a straight line during the deformation process) and assuming perfect bonding between laminae. The *in-plane* components of the (infinitesimal) strain tensor are interpolated and by making use of the constitutive law, the corresponding *in-plane* stress distribution is deduced for each layer. *Out-of-plane* shear stresses are then computed by integrating the equilibrium equations in each lamina, account taken of their continuity requirements. *Out-of-plane* shear strains are finally obtained via the inverse constitutive law.

The resulting global strain field depends on a fixed number of parameters, regardless of the total number of layers; 12 degrees of freedom are for instance assumed for the developed rectangular element.

The proposed model does not suffer locking phenomena even in the thin plate limit and provides an accurate description of inter-laminar stresses. Results are compared with both analytical and other finite element solutions.

keywords: Laminated composite plates, hybrid finite elements, assumed strain methods, shear-locking.

Introduction

Finite elements for the analysis of laminated composite plates have been derived by using different laminate theories proposed in the literature [see [32], and references quoted therein]. Such theories are usually referred to as:

- Equivalent Single Layer (ESL) theories, such as:
 - the Classical Lamination Theory (CLT) based on the Kirchhoff model;
 - the First-order Shear Deformation Theory (FSDT);

¹DIMS, University of Trento, Trento, ITALY; corresponding author.

²Italferr, Milano, ITALY.

³DI, University of Ferrara, Ferrara, ITALY.

⁴UCI, Irvine, CA, USA.

– Higher-order Shear Deformation Theories (HSDTs);

- Layer-wise Lamination Theory (LLT);
- Three dimensional elasticity.

In the context of ESL theories, the simplest one is the CLT which neglects the shear contribution in the laminate thickness. However, flat structures made of fiber-reinforced composite materials are characterized by non-negligible shear deformations in the thickness direction, since the longitudinal elastic modulus of the lamina can much higher than the shear and the transversal moduli; hence the use of a shear deformation laminate theory is recommended.

The extension of the [33] and [20] model to the case of laminated anisotropic plates, i.e. FSDT [[49]; [47]], accounts for shear deformation along the thickness in the simplest way. It gives satisfactory results for a wide class of structural problems, even for moderately thick laminates, requiring only C^0 -continuity for the displacement field. However in the classical FSDT:

- the *transverse shearing strains (stresses) are assumed to be constant* along the plate thickness so that stress boundary conditions on the top and the bottom of the plate are violated;
- *shear correction factors* must be introduced. The determination of shear correction factors is not a trivial task, since they depend both on the lamination sequence and on the state of deformation [see, e.g. [46]; [44]; [39]] and can be quite different from the value 5/6 which is typical of homogeneous plates.

Some methods have been proposed for improving FSDT results. For instance post-processing can be applied in order to improve the transverse shear stresses [viz. [21]; [35]], and the transverse normal stress [[36]; [52]] in finite element analysis.

Recently, refined FSDT models have been proposed: additive shear warping functions [24] or the assumption that shear strains vary in the thickness in cylindrical bending with the same law as the shear stress obtained by integrating the equilibrium equations [[29]; [3]] have been successfully employed.

More refined laminate theories are available, of course, and they can be broadly divided into the three groups outlined above.

On one hand, several ESL higher-order theories (and related finite elements models) have been proposed: within these theories, for instance, the transverse displacement has been either expanded in power series in terms of thickness coordinates up to a given order [[9]; [18]; [30]; [25]; [50]; [51]; [14]] or has been modelled by Legendre polynomials [[26]; [10]].

On the other hand, LLT [[31]; [11]; [34]; [5]] assumes a displacement representation formula in every layer.

Finally, analytical solutions based on three dimensional elasticity (and corresponding finite element models) have been developed, for instance, by [22]; [23]; [17].

All these higher-order theories lead to more accurate results, especially for very thick laminates. However the computational cost will be significantly increased [34], due to the increase of variables associated to either the description of the transversal displacement or the number of layers.

“To date, FSDT is still considered the best compromise between the capability for prediction and computational cost for a wide class of applications” [8].

With reference to finite element models, although it is usual to present FSDT within the framework of displacements approaches, nonetheless, in the literature, hybrid and mixed formulations have been proposed as well, mainly for developing innovative finite element models: see [1]; [27]. Assumed-stress four-node *single-layer* — i.e. homogeneous — plate elements have been developed since many years [[42]; [28]].

Four-node hybrid stress laminated elements including transverse shear effects have been developed by [19], where the stress field is defined separately for each layer and by [43], which, on the contrary, define the stress field for the laminate as a whole with inter-layer traction continuity and upper/lower laminate free surface conditions enforced exactly. The four-node hybrid stress multi-layer plate elements quoted above have the potential disadvantage of possessing two spurious zero energy modes. To overcome this problem, [41] developed an 8-node multi-layer laminated plate element for both thin and thick plates which has the correct rank and does not lock in the thin plate limit.

In all the above quoted papers, however, both the transverse (i.e. *out-of-plane*) and the *in-plane* stress components within the element are independently assumed. The interpolation functions, in order to enforce the inter-laminar continuity conditions, appear to be very complicated.

Finally it should be emphasized that new finite elements based on FSDT are still being proposed by many researchers [see e.g. the recent papers by [40]; [37]; [2]; [8]].

In this paper, a new four-node hybrid assumed-strain finite element for composite laminate plates is developed, which retains the basic assumptions of the FSDT: i.e. that particles of the plate originally lying along a straight line, which is normal to the undeformed middle surface, are assumed to remain aligned along a straight line during the deformation process, together with perfect bonding between laminae. The *in-plane* components of the strain tensor are interpolated and assumed to vary linearly along the thickness. By making use of the constitutive law, the

corresponding *in-plane* stress distribution is deduced for each layer whereas *out-of-plane* shear stresses are then computed by integrating the equilibrium equations in each lamina, account taken of their continuity requirements. *Out-of-plane* shear strains are finally obtained via the inverse constitutive law.

In this way the basic hypothesis of FSDT allows keeping a reasonably small number of strain parameters (which is, however, independent of the number of laminae), while preserving a sufficiently accurate description of inter-laminar stress distribution. Moreover it turns out that there is no need of *a priori* defining any shear-correction factor. In analogy with a recently developed non-symmetric hybrid stress assumed homogeneous plate element [12] the shear strain energy turns out to be *exactly* zero in the thin plate limit, and this prevents the occurrence of locking phenomena.

The organization of the paper is as follows: in section 2 the FSDT equations are presented in a way which is suitable for developing the formulation of the model. In Section 3 the four-node element is derived from a three-field hybrid-mixed variational principle, and in Section 4 the stiffness matrix is obtained. Finally, in Section 5, the performance of the new element is assessed with reference to meaningful benchmark problems, chosen in order to show its effectiveness and accuracy.

Laminated plates and FSDT

With the term laminate plate we refer to a thin (or moderately thick) flat body, constituted by K layers with different mechanical characteristics, stacked one above the other and occupying the domain:

$$\Omega = \left\{ (x_1, x_2, x_3) \in R^3 \mid x_3 \in [-h/2, +h/2], \right. \\ \left. (x_1, x_2) \in \tilde{\Omega} \subset R^2 \right\} \quad (1)$$

where the plane $\tilde{\Omega}$ (i.e. $x_3 = 0$) coincides with the middle surface of the undeformed plate, and the transverse dimension, whose thickness is h , is small compared to the other two dimensions, see Figure 1.

The layers are assumed to lie parallel to the middle surface $\tilde{\Omega}$; the typical k -th layer lies between the thickness coordinates h_{k-1} and h_k and is supposed to be orthotropic with material axes oriented at an angle θ^k with reference to the laminate coordinate x_1 .

The whole lateral surface of the body, $\partial\Omega$, is the union of the upper and lower faces Ω^+ and Ω^- and of the lateral surface Ω^L .

Symmetric laminate

Before discussing in detail the laminate kinematics and statics, it is useful to introduce the terminology associated with the particular lamination scheme considered. The lamination scheme of a laminate will be denoted by $[\alpha/\beta/\gamma/\delta/\varepsilon/\dots]$,

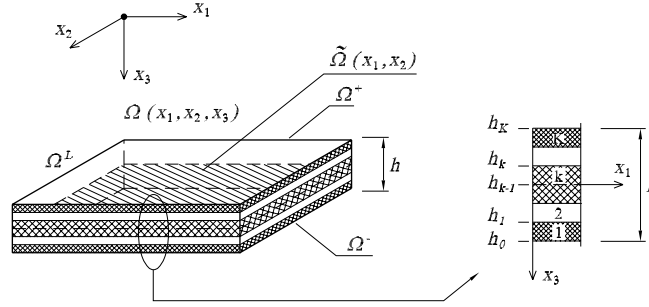


Figure 1: Coordinate system and layer numbering used for a typical laminated plate.

where α is the orientation of the first layer with reference to x_1 , β that of the second layer, and so on (see Figure 2).

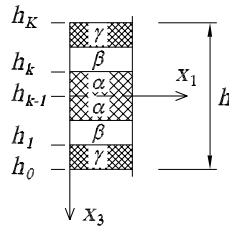


Figure 2: A symmetric laminate: lamination scheme $[\gamma/\beta/\alpha/\alpha/\beta/\gamma]_S = [\gamma/\beta/\alpha]_S$.

A laminate is said to be *symmetric* if the layer stacking sequence, the material properties and the geometry of the layers are symmetric with reference to the mid-plane, $\tilde{\Omega}$, of the laminate. Only the sequence relevant to laminae having a positive x_3 coordinate need to be prescribed since, by virtue of the above mentioned symmetry, the same sequence appears when moving on the negative side of the axis. From now on, only laminated plates satisfying a symmetric lamination scheme will be considered.

Load conditions

To avoid, for the sake of simplicity, stretching effects, loading on the plate upper and lower surfaces (bases) Ω^\pm is assumed to consist only of distribution of external surface loads f_3^\pm , acting along the x_3 -direction. For the same reason, the *in-plane* components of the body forces (b_1, b_2) are assumed to be zero within each lamina; whereas the *out-of-plane* (or transverse) component, b_3 , is assumed to be constant in each layer. An analogous hypothesis is adopted for the traction distributions applied to the lateral surface Ω^L .

As a consequence, by taking into account only the non-zero surface and body

forces, the following load condition is assumed:

$$f_3 = \tilde{f}_3^\pm \quad \text{on } \Omega^\pm \quad (2)$$

$$b_3^k = \tilde{b}_3^k \quad \text{on } \Omega \quad (3)$$

$$f_1^k = x_3 \tilde{f}_1^k, \quad f_2^k = x_3 \tilde{f}_2^k \quad \text{on } \Omega^L. \quad (4)$$

where the symbol $\tilde{}$ denotes a field defined on the middle surface, $\tilde{\Omega}$, being, therefore, a function of coordinates x_1, x_2 only.

Strain and stress fields

Let us assume the typical assumption of the Reissner-Mindlin and FSDT theories: particles of the plate originally lying along a straight line, which is normal to the undeformed middle surface, remain on a straight line during deformation, but this line is no more necessarily perpendicular to the deformed middle surface. Hence, the effects of shear deformations can be taken into account.

Thus, the *in-plane* strain components can be written as:

$$\varepsilon_{11} = x_3 \tilde{\varepsilon}_{11}(x_1, x_2) \quad (5)$$

$$\varepsilon_{22} = x_3 \tilde{\varepsilon}_{22}(x_1, x_2) \quad (6)$$

$$\varepsilon_{21} = \varepsilon_{12} = x_3 \tilde{\varepsilon}_{12}(x_1, x_2). \quad (7)$$

According to Eq. (5)–(7) the *in-plane* components of the strain tensor vary linearly along the thickness, as in the classical plate theory.

As a consequence, by making use of the Constitutive Law (CL) enforced at the local level for the k -th lamina, it turns out that the *in-plane* stress components ($\sigma_{11}^k, \sigma_{22}^k, \sigma_{12}^k = \sigma_{21}^k$) vary linearly along the transverse direction of the lamina, just like in the classical plate theories; however, in general, these components are discontinuous at the interface between two laminae having different orientation and/or material properties.

Since the single lamina is assumed to be thin, the stress component σ_{33}^k , which is perpendicular to the middle surface of the laminate, is assumed to vanish, as it is customary in the theory of homogeneous thin plates.

Moreover, for the sake of simplicity (even though an extension to the *monoclinic* case is straightforward) it is assumed that each lamina is *orthotropic*, so that its *in-plane* elastic behaviour is completely defined by four coefficients only; let $C_{11}^k, C_{12}^k, C_{22}^k, C_{66}^k$ be the independent components of the elastic tensor — written in the usual, compact notation dating back to Voigt — for the k -th lamina.

Then CL applied to Eqs. (5)–(7) yields:

$$\sigma_{11}^k = x_3 \tilde{\sigma}_{11}^k(x_1, x_2) = x_3 [C_{11}^k \tilde{\epsilon}_{11} + C_{12}^k \tilde{\epsilon}_{22}] \quad (8)$$

$$\sigma_{22}^k = x_3 \tilde{\sigma}_{22}^k(x_1, x_2) = x_3 [C_{12}^k \tilde{\epsilon}_{11} + C_{22}^k \tilde{\epsilon}_{22}] \quad (9)$$

$$\sigma_{12}^k = x_3 \tilde{\sigma}_{12}^k(x_1, x_2) = x_3 [2C_{66}^k \tilde{\epsilon}_{12}] \quad (10)$$

Looking at Eqs. (8)–(10), it should be remarked that the *in-plane* strain components do *not* depend on the k -th layer so that only a small number of parameters need to be introduced to completely describe the stress field within the plate.

Stress components are labelled in such a way that the former index denotes their direction, and the latter the normal to the face they are relevant to, and, as a shorthand notation, a comma denotes partial derivative with respect to the corresponding coordinate.

Thus, the Linear Momentum Balance (LMB) equations for the k -th layer read, account taken of Eq. (3):

$$\sigma_{11,1}^k + \sigma_{12,2}^k + \sigma_{13,3}^k = 0 \quad (11)$$

$$\sigma_{21,1}^k + \sigma_{22,2}^k + \sigma_{23,3}^k = 0 \quad (12)$$

$$\sigma_{31,1}^k + \sigma_{32,2}^k + b_3^k = 0. \quad (13)$$

By taking now into account the equilibrium equations (i.e. the LMB) in the x_1 and x_2 directions, the *out-of-plane* components of the stress field in the k -th layer, $\sigma_{31}^k = \sigma_{13}^k$, $\sigma_{32}^k = \sigma_{23}^k$ can be derived explicitly. It is useful to note that, while the Angular Momentum Balance (AMB) equation for the *in-plane* stress components, i.e. $\sigma_{12}^k = \sigma_{21}^k$, turns out to be satisfied as a consequence of the symmetry of the strain tensor, the AMB conditions for the *out-of-plane* stress components are *a priori* enforced, as it is customary in the classical theory of linear elasticity.

Eqs. (11)–(12) can be rewritten as:

$$\sigma_{13,3}^k = -x_3 (\tilde{\sigma}_{11,1}^k + \tilde{\sigma}_{12,2}^k) \quad (14)$$

$$\sigma_{23,3}^k = -x_3 (\tilde{\sigma}_{21,1}^k + \tilde{\sigma}_{22,2}^k). \quad (15)$$

Then the *out-of-plane* shear components can be obtained as follows:

$$\sigma_{13}^k = \sigma_{13}^{0,k} - \int_{-h/2}^{x_3} x_3 (\tilde{\sigma}_{11,1}^k + \tilde{\sigma}_{12,2}^k) dx_3 \quad (16)$$

$$\sigma_{23}^k = \sigma_{23}^{0,k} - \int_{-h/2}^{x_3} x_3 (\tilde{\sigma}_{21,1}^k + \tilde{\sigma}_{22,2}^k) dx_3, \quad (17)$$

where $\sigma_{13}^{0,k}$, $\sigma_{23}^{0,k}$ are integration constants.

Traction Boundary Conditions (TBCs) require that both σ_{13} and σ_{23} must vanish on the plate bases Ω^\pm ; they are simply satisfied by setting $\sigma_{13}^I(h_0) = 0$, $\sigma_{23}^I(h_0) = 0$ and $\sigma_{13}^K(h_K) = 0$, $\sigma_{23}^K(h_K) = 0$, where indices I and K refer obviously to the bottom and top layers respectively, as shown in Figure 1.

Therefore it results, for the first layer:

$$\sigma_{13}^I = -\frac{1}{2}(x_3^2 - h_0^2)(\tilde{\sigma}_{11,1}^I + \tilde{\sigma}_{12,2}^I) \quad (18)$$

$$\sigma_{23}^I = -\frac{1}{2}(x_3^2 - h_0^2)(\tilde{\sigma}_{21,1}^I + \tilde{\sigma}_{22,2}^I), \quad (19)$$

and for the k -th layer:

$$\sigma_{13}^k = \sigma_{13}^{0,k} - \frac{1}{2}(x_3^2 - h_{k-1}^2)(\tilde{\sigma}_{11,1}^k + \tilde{\sigma}_{12,2}^k) \quad (20)$$

$$\sigma_{23}^k = \sigma_{23}^{0,k} - \frac{1}{2}(x_3^2 - h_{k-1}^2)(\tilde{\sigma}_{21,1}^k + \tilde{\sigma}_{22,2}^k), \quad (21)$$

where the explicit form of the integration constants $\sigma_{13}^{0,k}$ and $\sigma_{23}^{0,k}$ is:

$$\sigma_{13}^{0,k} = \sum_{\ell=1}^{k-1} -\frac{1}{2}(h_\ell^2 - h_{\ell-1}^2)(\tilde{\sigma}_{11,1}^\ell + \tilde{\sigma}_{12,2}^\ell) \quad (22)$$

$$\sigma_{23}^{0,k} = \sum_{\ell=1}^{k-1} -\frac{1}{2}(h_\ell^2 - h_{\ell-1}^2)(\tilde{\sigma}_{21,1}^\ell + \tilde{\sigma}_{22,2}^\ell). \quad (23)$$

Once the transverse shear stresses are known, by making use of the inverse CL the corresponding *out-of-plane* shear strain components can be evaluated: if, according to the usual notation, C_{44}^k and C_{55}^k are the relevant components of the elastic tensor for the k -th lamina, then:

$$\varepsilon_{13}^k = \frac{\sigma_{13}^k}{2C_{55}^k} \quad (24)$$

$$\varepsilon_{23}^k = \frac{\sigma_{23}^k}{2C_{44}^k} \quad (25)$$

Displacement field

The in-plane component (u_1 , u_2) of the displacement field are assumed, analogously to the classical Reissner-Mindlin model, to vary linearly along the transverse direction of the laminated plate, while the normal component, u_3 , is assumed to be

constant along the x_3 -axis:

$$u_1(x_1, x_2, x_3) = -x_3 \tilde{\varphi}_1(x_1, x_2) \quad (26)$$

$$u_2(x_1, x_2, x_3) = -x_3 \tilde{\varphi}_2(x_1, x_2) \quad (27)$$

$$u_3(x_1, x_2, x_3) = \tilde{u}_3(x_1, x_2). \quad (28)$$

Here $\tilde{\varphi}_1$ and $\tilde{\varphi}_2$ are the rotations (see Figure 3) of the transverse line elements, which initially lie perpendicular to the middle surface, about the x_1 - and x_2 -axes.

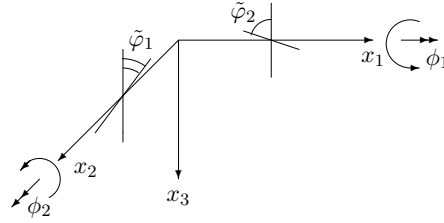


Figure 3: Rotations of the transverse line element of the plate $\tilde{\varphi}_1$ and $\tilde{\varphi}_2$ used in the present formulation and corresponding Cartesian components, ϕ_1 and ϕ_2 , of the infinitesimal rotation vector.

Variational formulation

In this Section a brief deduction of assumed-strain hybrid finite elements is presented. A 3-D continuum is considered, occupying a volume Ω , bounded by a smooth surface $\partial\Omega = \partial\Omega_u \cup \partial\Omega_s$, with $\partial\Omega_u \cap \partial\Omega_s = \emptyset$; $\partial\Omega_u$ is the portion of the boundary where the displacement field is prescribed, whereas $\partial\Omega_s$ is the complementary part of the boundary, where TBCs must be fulfilled.

Let us assume the following three-field variational principle (often credited to Hu-Washizu, see [45]):

$$\begin{aligned} \Pi_{HW}(\sigma_{ij}, \varepsilon_{ij}, u_i) &= \frac{1}{2} \int_{\Omega} (C_{ijmn} \varepsilon_{ij} \varepsilon_{mn} - b_i u_i) dV \\ &\quad - \int_{\Omega} \sigma_{ij} [\varepsilon_{ij} - \frac{1}{2} (u_{i,j} + u_{j,i})] dV \\ &\quad - \int_{\partial\Omega_s} f_i u_i dS - \int_{\partial\Omega_u} \sigma_{ij} n_j (u_i - \bar{u}_i) dS. \end{aligned} \quad (29)$$

In Eq. (29) C_{ijmn} , σ_{ij} , ε_{ij} , u_i denote, respectively, the Cartesian components of the fourth-order elasticity tensor, of the second-order stress and strain tensors and of the displacement vector; b_i and f_i denote the components of body and surface forces respectively, while \bar{u}_i are the prescribed displacement components.

It can be easily shown that the stationarity conditions of functional (29), when AMB is *a priori* satisfied, provide the following field equations:

- LMB: $\sigma_{ij,j} + b_i = 0$ in Ω ;
- CC: $\varepsilon_{ij} = u_{i,j}^S$ in Ω ;
- CL: $\sigma_{ij} = C_{ijmn}\varepsilon_{mn}$ in Ω ;
- TBC: $\sigma_{ij}n_j = f_i$ on $\partial\Omega_s$;
- DBC: $u_i = \bar{u}_i$ on $\partial\Omega_u$,

where CC stands for Compatibility Condition, and DBC for Displacement Boundary Condition; whereas $u_{i,j}^S = \frac{1}{2}(u_{i,j} + u_{j,i})$ is the symmetric part of the displacement gradient.

If CL is *a priori* enforced, then it is possible, by applying also the divergence theorem, to eliminate the stress components from Eq. (29), obtaining this *modified* Hu-Washizu functional, depending only on strain and displacement fields:

$$\begin{aligned}
\Pi_{HW,mod}(\varepsilon_{ij}, u_i) &= -\frac{1}{2} \int_{\Omega} C_{ijmn} \varepsilon_{ij} \varepsilon_{mn} dV \\
&\quad - \int_{\Omega} (C_{ijmn} \varepsilon_{mn,j} + b_i) u_i dV \\
&\quad + \int_{\partial\Omega_s} (C_{ijmn} \varepsilon_{mn} n_j - f_i) u_i dS \\
&\quad + \int_{\partial\Omega_u} C_{ijmn} \varepsilon_{mn} n_j \bar{u}_i dS.
\end{aligned} \tag{30}$$

If, instead of a continuous homogeneous solid, a laminated body is considered, which satisfies the previously introduced hypotheses about geometry, Eq. (1), loads, Eqs. (2)–(4), strain distribution, Eqs. (5)–(7) and (24)–(25), the variational principle (30) must be modified accordingly:

$$\begin{aligned}
\Pi_{HW,mod}(\varepsilon_{ij}, u_i) &= \sum_{k=1}^K \left[-\frac{1}{2} \int_{\hat{\Omega}} C_{ijmn}^k \int_{h_{k-1}}^{h_k} \varepsilon_{ij}^k \varepsilon_{mn}^k dx_3 dA \right. \\
&\quad - \int_{\hat{\Omega}} (C_{ijmn}^k \int_{h_{k-1}}^{h_k} \varepsilon_{mn,j}^k u_i dx_3 + \hat{b}_3 u_3) dA \\
&\quad \left. + \int_{\Omega^L} C_{ijmn}^k \int_{h_{k-1}}^{h_k} \varepsilon_{mn}^k n_j \bar{u}_i dx_3 dl \right],
\end{aligned} \tag{31}$$

where, for the sake of simplicity, a laminated plate with *only* prescribed DBCs on its boundary Ω^L has been considered, so that the external load contribution, \hat{b}_3 , is defined as follows:

$$\hat{b}_3 = \sum_{k=1}^K \tilde{b}_3^k (h_k - h_{k-1}) + \tilde{f}_3^+ + \tilde{f}_3^-. \tag{32}$$

Functional (31) can be easily modified to cope with the case when also TBCs are given on a portion of the plate boundary Ω^L .

For a hybrid type laminate element, the discretized version of functional (31) is:

$$\begin{aligned} \Pi_{HW,mod}^{H,e}(\varepsilon_{ij}, u_i, \hat{u}_i) = & \sum_{k=1}^K \left[-\frac{1}{2} \int_{\tilde{\Omega}^e} C_{ijmn}^k \int_{h_{k-1}}^{h_k} \varepsilon_{ij}^k \varepsilon_{mn}^k dx_3 dA \right. \\ & - \int_{\tilde{\Omega}^e} (C_{ijmn}^k \int_{h_{k-1}}^{h_k} \varepsilon_{mn,j}^k u_i dx_3 + \hat{b}_3 u_3) dA \\ & \left. + \int_{\Omega^{L^e}} C_{ijmn}^k \int_{h_{k-1}}^{h_k} \varepsilon_{mn}^k n_j \hat{u}_i dx_3 dl \right], \end{aligned} \quad (33)$$

where \hat{u}_i is a displacement field defined only on the boundary Ω^{L^e} of the e -th element, whose domain is $\tilde{\Omega}^e$.

The finite element model

The starting point to derive a Hybrid Assumed-Strain Laminate (or briefly, HASL) model [see, for instance, [7]] for the Reissner-Mindlin plate consists in enforcing the stationarity conditions of the previously introduced mixed-hybrid functional (33). Let us subdivide the plate mid-surface, $\tilde{\Omega}$, into M sub-domains, $\tilde{\Omega}^e$, such that $\tilde{\Omega} \cong \cup^e \tilde{\Omega}^e$.

A simple quadrilateral 12 degrees-of-freedom (dofs) laminated plate with constant thickness can be developed as follows (see Figure 4).

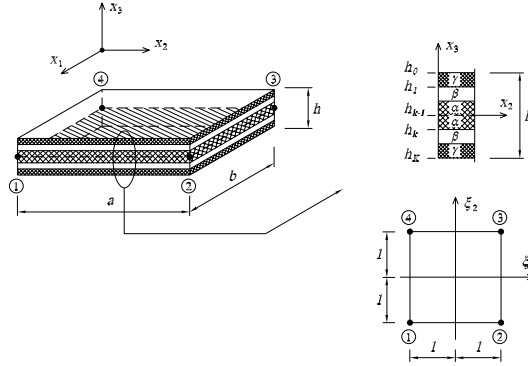


Figure 4: The rectangular Hybrid Assumed-Strain Laminated element (HASL).

Let us assume a local reference system (x_1, x_2, x_3) , where the x_1 - and x_2 -axes are aligned with the 1-2 and 1-4 sides respectively, and the x_3 -axis is determined by the right-hand rule. A plane natural reference system (ξ_1, ξ_2) , with $-1 \leq \xi_i \leq 1$ ($i=1, 2$) is then introduced [see, for instance [53]; [15]; [4]] and is related to the local one by the following relationships (as in standard isoparametric elements):

$$x_i(\xi_i) = \sum_{\ell=1}^4 N^\ell(\xi_i) x_i^\ell \quad (34)$$

where x_i^ℓ , (with $\ell = 1, \dots, 4$), are the nodal coordinates of the element, while $N^\ell(\xi_i)$ are the shape functions given by:

$$N^\ell(\xi_i) = \frac{1}{4}(1 + \xi_1 \xi_1^\ell)(1 + \xi_2 \xi_2^\ell) \quad (\ell = 1, \dots, 4). \quad (35)$$

The nodal coordinates in the natural reference system are, of course, given by $(\xi_1, \xi_2) = (\pm 1, \pm 1)$.

The strain field

With reference to the natural reference system ξ_1, ξ_2 (see Figure 4), let us assume the following *in-plane* components of the strain tensor ε_{ij}^* :

$$\varepsilon_{11}^{*k} = \varepsilon_{11}^* = x_3 \tilde{\varepsilon}_{11}^* = x_3(\alpha_0 + \alpha_1 \xi_1 + \alpha_2 \xi_2) \quad (36)$$

$$\varepsilon_{22}^{*k} = \varepsilon_{22}^* = x_3 \tilde{\varepsilon}_{22}^* = x_3(\beta_0 + \beta_1 \xi_1 + \beta_2 \xi_2) \quad (37)$$

$$\varepsilon_{12}^{*k} = \varepsilon_{12}^* = x_3 \tilde{\varepsilon}_{12}^* = x_3(\gamma_0 + \gamma_1 \xi_1^2 + \gamma_2 \xi_2^2). \quad (38)$$

A strain vector β is then introduced, as a short-hand notation, to collect component-wise the above introduced strain parameters:

$$\beta = \{\alpha_0, \alpha_1, \alpha_2, \beta_0, \beta_1, \beta_2, \gamma_0, \gamma_1, \gamma_2\}^T. \quad (39)$$

The *in-plane* stress components, corresponding to the *in-plane* strain components (36)–(38), are given, for the generic k -th layer, by Eqs. (8)–(10). By substituting (36)–(38) into (8)–(10), one obtains the following stress components, expressed in the natural reference system:

$$\sigma_{11}^k = x_3 [C_{11}^k(\alpha_0 + \alpha_1 \xi_1 + \alpha_2 \xi_2) + C_{12}^k(\beta_0 + \beta_1 \xi_1 + \beta_2 \xi_2)] \quad (40)$$

$$\sigma_{22}^k = x_3 [C_{21}^k(\alpha_0 + \alpha_1 \xi_1 + \alpha_2 \xi_2) + C_{22}^k(\beta_0 + \beta_1 \xi_1 + \beta_2 \xi_2)] \quad (41)$$

$$\sigma_{12}^k = x_3 [2C_{66}^k(\gamma_0 + \gamma_1 \xi_1^2 + \gamma_2 \xi_2^2)]. \quad (42)$$

The *out-of-plane* components $\sigma_{13}^k, \sigma_{23}^k$ (referred again to the natural reference system) can be determined by making use of the LMB equations, as shown in Section 2.3; for the assumed strain interpolations (36)–(38), Eqs. (14)–(15) provide:

$$\sigma_{13}^k = -\frac{1}{2}(x_3^2 - h_{k-1}^2)[(C_{11}^k \alpha_1 + C_{12}^k \beta_1) + C_{66}^k(4\gamma_2 \xi_2)] + \sigma_{13}^{0,k} \quad (43)$$

$$\sigma_{23}^k = -\frac{1}{2}(x_3^2 - h_{k-1}^2)[(C_{12}^k \alpha_2 + C_{22}^k \beta_2) + C_{66}^k(4\gamma_1 \xi_1)] + \sigma_{23}^{0,k}, \quad (44)$$

where the integration constants $\sigma_{13}^{0,k}$, $\sigma_{23}^{0,k}$ are defined exactly as in Eqs. (22)–(23).

Similarly, the *out-of-plane* strain components ε_{13}^{*k} , ε_{23}^{*k} are computed by Eqs. (24)–(25).

It should be remarked that if a linear interpolation is assumed for the *in-plane* shear strain components, $\tilde{\varepsilon}_{12}^* = \tilde{\varepsilon}_{21}^*$ — instead of the adopted incomplete quadratic one, Eq. (38) — the *out-of-plane* shear stress components, $\tilde{\sigma}_{13}^k$ and $\tilde{\sigma}_{23}^k$ turn out to be constant along both the ξ_1 and the ξ_2 direction, providing a too stiff element [see [12]].

Finally, the Cartesian strain components of the k -th lamina, ε_{ij}^{*k} defined in the natural reference system need to be expressed in the local (or physical) reference system; the corresponding Cartesian components, ε_{ij}^k are defined by the following transformation rule:

$$\varepsilon_{mn}^k = J_{im} \varepsilon_{ij}^{*k} J_{jn}, \quad (45)$$

where J_{im} denotes the elements of the Jacobian matrix of the isoparametric transformation (34); see for instance [7].

Even though the formulation can be extended to cover the case of distorted element, only simple cases — like the rectangular one — where the Jacobian of the element is constant (and therefore coincides with its value at the centroid) will be discussed here.

The displacement field

In the following, the displacement field can be conveniently expressed in terms of the transverse displacements \tilde{u}_3^ℓ ($\ell = 1, \dots, 4$) and of the rotations $\tilde{\varphi}_i^\ell$ (with $i = 1, 2$) of transverse line elements, evaluated at the four nodes of the plate.

The components of the assumed displacement field are then functions of these nodal dofs and are expressed in terms of the shape functions (34) as follows:

$$u_1 = -x_3 \sum_{\ell=1}^4 N^\ell(\xi_i) \tilde{\varphi}_1^\ell \quad (46)$$

$$u_2 = -x_3 \sum_{\ell=1}^4 N^\ell(\xi_i) \tilde{\varphi}_2^\ell \quad (47)$$

$$u_3 = \sum_{\ell=1}^4 N^\ell(\xi_i) \tilde{u}_3^\ell. \quad (48)$$

As a short-hand notation, the following generalized nodal displacement vector is introduced:

$$\mathbf{q} = \{ \tilde{u}_3^1, \tilde{\varphi}_1^1, \tilde{\varphi}_2^1, \tilde{u}_3^2, \tilde{\varphi}_1^2, \tilde{\varphi}_2^2, \tilde{u}_3^3, \tilde{\varphi}_1^3, \tilde{\varphi}_2^3, \tilde{u}_3^4, \tilde{\varphi}_1^4, \tilde{\varphi}_2^4 \}^T. \quad (49)$$

It should be remarked that in the HASL element, the displacement field components \hat{u}_i ($i = 1, 2, 3$), occurring in Eq. (33) are defined by the same shape functions (46)–(48), but need to be defined only on the element edges $\xi_1 = \pm 1$ and $\xi_2 = \pm 1$.

The finite element stiffness matrix

The stiffness matrix \mathbf{K} of the HASL element is derived by substituting the interpolation fields defined in the previous Sections 4.1 and 4.2 into the modified Hu-Washizu functional (33).

The two independently discretized fields of displacements u_i , \hat{u}_i and strains, ε_{ij} written in the physical reference system x_i ($i = 1, 2, 3$) of the finite element read as follows:

$$u_i(x_i) = \mathbf{N}_u(x_i)\mathbf{q} \quad (50)$$

$$\varepsilon_{ij}(x_i) = \mathbf{N}_\varepsilon(x_i)\boldsymbol{\beta}, \quad (51)$$

where $\mathbf{N}_u(x_i)$ denotes the matrix of the shape functions for the displacement field (46)–(48); $\mathbf{N}_\varepsilon(x_i)$ denotes the matrix of the shape functions for the strain field (36)–(38), whereas the corresponding vectors \mathbf{q} , $\boldsymbol{\beta}$ are defined in Eqs. (49) and (39).

Substitution of Eqs. (50) and (51) into (33) yields the following discretized variational principle:

$$\Pi_{HW,mod}^{H,e} = -\frac{1}{2}\boldsymbol{\beta}^T \mathbf{H}_{\beta\beta} \boldsymbol{\beta} + \boldsymbol{\beta}^T \mathbf{G}\mathbf{q} - \mathbf{F}^T \mathbf{q}, \quad (52)$$

where:

$$\boldsymbol{\beta}^T \mathbf{H}_{\beta\beta} \boldsymbol{\beta} = \sum_k \left[\int_{\tilde{\Omega}^e} C_{ijmn}^k \int_{h_{k-1}}^{h_k} \varepsilon_{ij}^k \varepsilon_{mn}^k dx_3 dA \right]; \quad (53)$$

$$\begin{aligned} \boldsymbol{\beta}^T \mathbf{G}\mathbf{q} = & \sum_k \left[- \int_{\tilde{\Omega}^e} C_{ijmn}^k \int_{h_{k-1}}^{h_k} \varepsilon_{mn,j}^k u_i dx_3 dA \right. \\ & \left. + \int_{\Omega^L} C_{ijmn}^k \int_{h_{k-1}}^{h_k} \varepsilon_{mn}^k n_j \hat{u}_i dx_3 dl \right]; \end{aligned} \quad (54)$$

$$\mathbf{F}^T \mathbf{q} = \int_{\tilde{\Omega}^e} \hat{b}_3 u_3 dA. \quad (55)$$

All the above integrals, defined in the physical configuration, are evaluated, with the usual techniques employed in isoparametric formulation, on the reference (i.e. natural) configuration.

It should be outlined that the first term on the right-hand side of Eq. (52) represents (to within the sign) the element strain energy, U^e , as it clearly appears in Eq. (53). In the present context, by virtue of the symmetric lamination scheme and

of the load conditions (2)–(4), it can be shown that the strain energy can be written as $U^e = U_b^e + U_s^e$ i.e. it splits into two contributions, the former, U_b^e , due to bending stresses, the latter, U_s^e , to transverse (or *out-of-plane*) shear stresses.

The strain energy due to these transverse shear stresses — see Eqs. (24)–(25) and (45) — is given by:

$$U_s^e = \sum_k \int_{\tilde{\Omega}^e} \int_{h_{k-1}}^{h_k} 2 \left[C_{55}^k (\boldsymbol{\varepsilon}_{13}^k)^2 + C_{44}^k (\boldsymbol{\varepsilon}_{23}^k)^2 \right] dx_3 dA, \quad (56)$$

and, with a procedure similar to that adopted in [12] it follows that when $h \rightarrow 0$, then $U_s^e \rightarrow 0$ like h^5 . Since it can be proven, with the same method, that the bending strain energy U_b^e is a cubic function of the laminate thickness h , when thickness becomes smaller and smaller, the shear strain energy U_s^e is negligible if compared to the bending strain energy, i.e. the ratio U_s^e/U_b^e goes to zero with the correct order in the thin plate limit.

By invoking now the stationarity conditions of $\Pi_{HW,mod}^{H,e}$ with reference to $\boldsymbol{\beta}$ and \mathbf{q} , the following system of simultaneous linear algebraic equations is obtained:

$$\begin{bmatrix} -\mathbf{H}_{\beta\beta} & \mathbf{G} \\ \mathbf{G}^T & \mathbf{O} \end{bmatrix} \begin{Bmatrix} \boldsymbol{\beta} \\ \mathbf{q} \end{Bmatrix} = \begin{Bmatrix} \mathbf{0} \\ \mathbf{F} \end{Bmatrix}. \quad (57)$$

By making use of static condensation techniques on $\boldsymbol{\beta}$, the following discrete equilibrium equations are obtained from Eq. (57):

$$\mathbf{K}\mathbf{q} = \mathbf{F}, \quad (58)$$

where the stiffness matrix \mathbf{K} appearing in Eq. (58) can be evaluated as follows:

$$\mathbf{K} = \mathbf{G}^T \mathbf{H}_{\beta\beta}^{-1} \mathbf{G}. \quad (59)$$

In this way, when the strain parameters are eliminated at the element level, at the assembly stage the element has exactly the same number and type of dofs as a standard displacement-based one. For this reason, the solution procedure is that of a standard stiffness formulation, and it is allowed mixing an element of this type with displacement-formulated ones.

For the HASL element under consideration — dual hybrid, according to [6] — matrix $\mathbf{H}_{\beta\beta}$ has to be positive-definite in order to satisfy the ellipticity condition, and this is verified for the assumed strain shape functions, as it can be checked. Therefore it is possible to evaluate $\boldsymbol{\beta}$ element by element, once the nodal displacement values \mathbf{q} are known, by the following equation:

$$\boldsymbol{\beta} = \mathbf{H}_{\beta\beta}^{-1} \mathbf{G}\mathbf{q}. \quad (60)$$

The discrete inf-sup condition for dual-hybrid methods can be verified by performing a singular value decomposition of matrix \mathbf{K} , see [48]; [13]. With the assumed strain distribution only the three zero eigenvalues corresponding to the three rigid body motions are found.

Numerical examples

Several numerical examples are discussed for both thick and thin laminated plates to evaluate the performances of the presented element.

The obtained results are compared with those available in the technical literature and with the solutions provided by the commercial finite element code ANSYS version 5.3: brick elements with assigned material properties have been used to model each layer.

In particular, results provided by the following elements have been reported: the partial-mixed models EML4 by [2]; the Partial-Hybrid Stress Laminated plate (denoted here by PHSL) by [51]; the isoparametric displacement-based elements QUAD4 and QUAD9 by [53]; the CTMQ20 Timoshenko-Mindlin quadrilateral finite element with 20 dofs by [8]; the Discrete Shear Triangular (DST) plate-bending element by [16]; the REC56-Z0 (with 56 dofs) and REC72-Z0 (with 72 dofs) elements by [37]. Finally, where it has been possible, analytical series solutions given for the 3-D case by [22] and for the 2-D case (i.e. corresponding to FSDT) by [32] have been reported, along with the *Higher order* laminated plate solutions by [18].

The following material constants have been used for all the considered examples:

$$E_1/E_2 = 25; \quad G_{12} = G_{13} = 0.5E_2; \quad G_{23} = 0.2E_2; \\ \nu_{12} = \nu_{13} = 0.25,$$

corresponding to a high-modulus orthotropic graphite-epoxy composite material.

1-D analysis of laminated plate

As a preliminary series of test, some cylindrical bending problems are considered: a laminated cantilever plate is constrained in such a way that its behavior is equivalent to that of a cantilever beam.

Cantilever laminated plate under tip line-load

The first considered problem is a four-layer [0/90/90/0] laminated cantilever plate subjected to a shear load applied to the free end (see Figure 5).

Each layer has equal thickness $h/4$; a one-element discretization and a four-elements discretization have been considered (see Figure 5a and 5b). Results have been compared with those provided by the 2-D analytical FSDT solution.

Table 1 shows the deflection at the free end of the laminate element for different thickness values. Results are expressed in normalized form, by dividing the

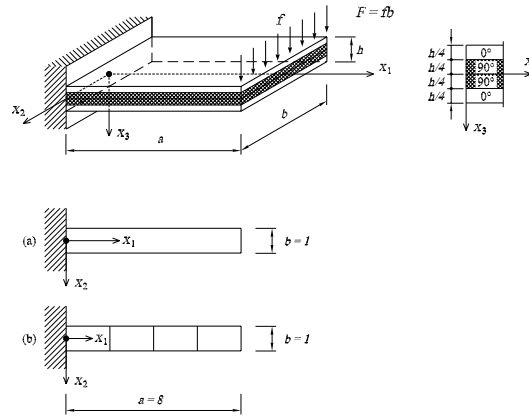


Figure 5: Four-layer laminated cantilever plate under shear load at the free end. (a) One element discretization; (b) Four elements discretization.

numerical results by the theoretical one, provided in [32] [Table 4.3.1, page 193]. It should be noticed that for all thickness values the results are in excellent agreement with those of the analytical solution and no locking phenomena are encountered.

Table 1: Normalized deflection, u_3 , at the free end of a laminated [0/90/90/0] cantilever plate under tip line-load

a/h	el.	1000	100	10	1
HASL	1	1.002	1.002	1.001	0.992
HASL	4	1.002	1.002	1.001	0.993
FSDT	—	1.000	1.000	1.000	1.000

Figure 6 presents the distribution of the shear stress $\sigma_{13}(x_3)$ for the problem under consideration (with $a/h = 1$), produced by the ANSYS code when a finite element analysis with eight-noded brick elements is performed.

Figure 7 shows instead the profile of the shear stress $\sigma_{13}(x_3)$ for the one-element discretization (again in the case $a/h = 1$), which is compared with the one provided by the finite element analysis already performed with brick elements.

It should be noticed that in any standard laminate theory (viz. CLT or FSDT), as in the present HASL model, the shear stress distribution does not vary along the x_1 -axis, whereas the 3-D solution (and, consequently, the finite element result produced by solid brick elements) takes into account the boundary-layer effects [see [38]] and therefore exhibits a different behavior close to the boundary (i.e for $x_1 = 0.5$) and in a generic section like that, here considered, defined by $x_1 = 6.5$.

As it is expected, the element shows a good ability to compute in a satisfactory way the *through-the-thickness* and inter-laminar shear stress, by satisfying exactly

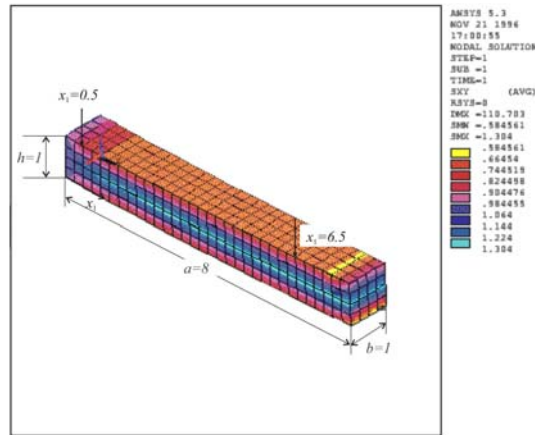


Figure 6: Distribution of shear stress σ_{13} for the [0/90/90/0] laminated plate (with $a/h = 1$) subjected to tip line-load, analyzed with brick elements: the finite element mesh is also shown.

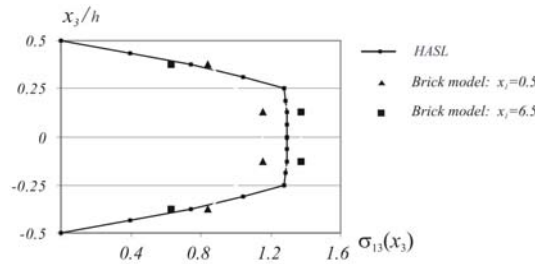


Figure 7: Distribution of shear stress σ_{13} along the thickness for the [0/90/90/0] laminated plate ($a/h = 1$) under tip line-load: comparison between HASL and brick model results.

both inter-laminar and top and bottom equilibrium conditions.

Cantilever laminated plate under uniformly distributed load

The second 1-D test is a four-layer [0/90/90/0] laminated cantilever plate subjected to a uniform load acting on the top surface Ω^+ (see Figure 8). As in the previous problem each layer has equal thickness ($h/4$).

Again, two different discretizations have been considered, one consisting of four elements, the other of eight elements; results, in terms of normalized tip deflection, have been compared with those provided by the FSDT analysis, which provides a reference solution given by [32] [Table 4.3.1, page 193].

These results in terms of normalized tip deflection at the middle surface of the HASL element are given in Table 2. The results are compared with the FSDT solution for several values of the depth-to-thickness ratio. Figure 9 presents the distribution of the shear stress $\sigma_{13}(x_3)$ for the problem under consideration (with

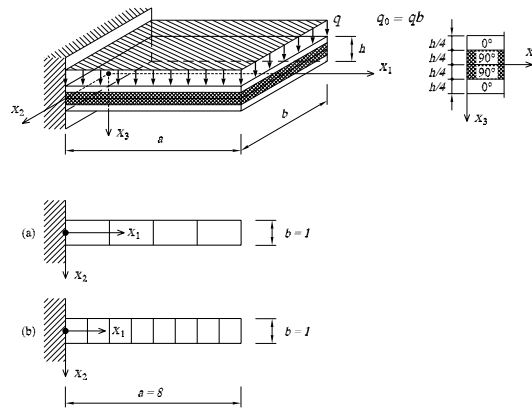


Figure 8: Four-layer laminated cantilever plate under uniformly distributed load. (a) Four elements discretization; (b) Eight elements discretization.

Table 2: Normalized deflection u_3 at the free end of a laminated $[0/90/90/0]$ cantilever plate under uniformly distributed load acting on the upper surface.

a/h	el.	1000	100	10	1
HASL	4	1.022	1.022	1.022	1.005
HASL	8	1.007	1.007	1.007	0.994
FSDT	—	1.000	1.000	1.000	1.000

$a/h = 1$), produced by a finite element analysis performed with eight-noded brick elements.

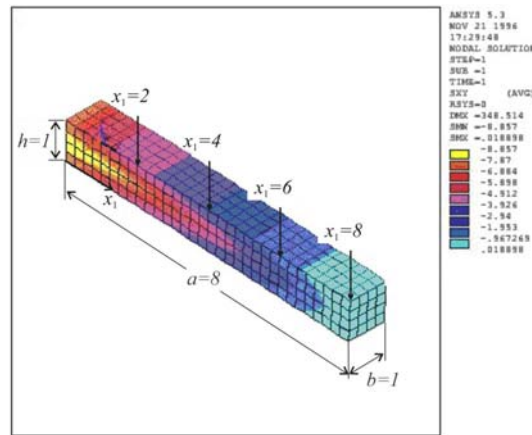


Figure 9: Distribution of shear stress σ_{13} for the $[0/90/90/0]$ laminated plate (with $a/h = 1$) subjected to uniformly distributed load, analyzed with ANSYS brick elements: the finite element mesh is also shown.

Figure 10 shows the shear stress profile $\sigma_{13}(x_3)$ for the 4-elements discretization (in the case $a/h = 1$) which is compared with the one produced by a brick finite element analysis.

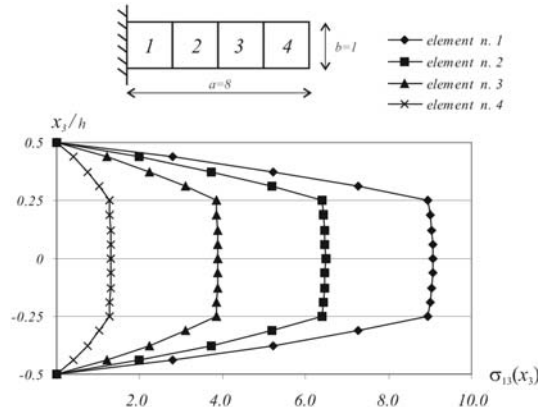


Figure 10: Distribution of shear stress σ_{13} along the thickness for the [0/90/90/0] laminated plate ($a/h = 1$) under uniformly distributed load: comparison between HASL and brick model results.

It should be noticed that, while in the HASL model the shear stress is constant along the x_1 - and x_2 -axes in *each element*, this does not happen in the brick model: for this reason the stress profiles which are relevant to several values of the x_1 coordinate are shown. Obviously, also in this case boundary layer affects are taken into account in the 3-D solution only, as shown in [38].

Composite laminate plates

In order to establish the performance of the proposed element in a truly 2-D environment, a simply-supported square laminated plate has been considered. The plate side length is denoted by a , whereas its thickness is h . The following boundary conditions have been adopted (corresponding to *hard boundaries*):

$$\begin{aligned} @ x_1 = 0 \text{ and } x_1 = a: & \quad u_2 = u_3 = 0, \quad \varphi_1 = 0 \\ @ x_2 = 0 \text{ and } x_2 = a: & \quad u_1 = u_3 = 0, \quad \varphi_2 = 0. \end{aligned}$$

The symmetric three-layer (i.e. [0/90/0]) and four-layer (i.e. [0/90/90/0]) cross-ply laminates have been separately considered, as shown in Figure 11.

The plate has been loaded either by a uniformly distributed load (UDL), q_0 , or by a doubly-sinusoidal load (SSL), $q = q_0 \sin(\pi x_1/a) \sin(\pi x_2/a)$, acting on the upper surface, Ω^+ .

Due to geometric and loading symmetry only a quarter of the plate was studied, and different meshes were adopted.

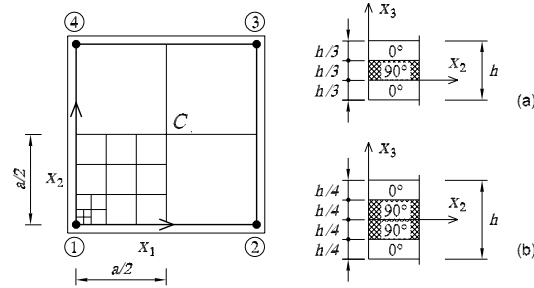


Figure 11: Simply-supported square laminated plate under distributed loads: the pattern of mesh refinement is partially shown. In (a) the [0/90/0] three-layer laminate is shown, in (b) the [0/90/90/0] four-layer one.

Symmetric [0/90/0] cross-ply laminated plate

In this case, shown in Figure 11a, the following normalization of the deflection of the plate center has been used when presenting the results [see Table 7.2.1, page 385 in [32]]:

$$\bar{u}_3 = \frac{100E_2h^3}{q_0a^4}u_3. \quad (61)$$

UDL: Uniformly distributed load

Table 3 presents the normalized transversal displacement at the plate center for the considered load case. For comparison purposes, the FSDT analytical solution and the results obtained by the hybrid 4-node (EML4) and the isoparametric displacement-based 4-node (QUAD4) and 9-node (QUAD9) elements are reported as well.

SSL: Double sinusoidally distributed load

Table 4 reports the normalized transversal deflection at the plate center for the present load case. Analogously as before, the analytical solution and some results available in the literature are presented for comparison purposes.

Symmetric [0/90/90/0] cross-ply laminated plate

The considered case is shown in Figure 11b; as before the two load conditions are considered separately.

UDL: Uniformly distributed load

The same normalized displacement given by Eq. (61) is used here in the presentation of results. Table 5 provides the normalized deflection at the plate center for the considered load case.

For comparison purposes, the FSDT analytical solution and the results obtained by ANSYS with the shell 99 element are reported as well.

In Figure 12 the distribution of *out-of plane* shear stresses $\sigma_{13}(x_3)$ and $\sigma_{23}(x_3)$

Table 3: Normalized deflection, u_3 , measured at the center of a simply-supported square laminated [0/90/0] plate under UDL.

a/h	mesh	100	10
HASL	3×3	0.6756	1.0445
	6×6	0.6711	1.0293
	12×12	0.6700	1.0262
EML4	3×3	—	1.0235
	6×6	—	1.0223
	12×12	—	1.0220
QUAD4	3×3	—	1.0331
	6×6	—	1.0243
	12×12	—	1.0225
QUAD9	6×6	—	1.0222
	12×12	—	1.0219
<i>FSDT</i>	—	0.6697	1.0219

Table 4: Normalized deflection, u_3 , measured at the center of a simply-supported square laminated [0/90/0] plate under SSL.

a/h	mesh	100	20	10
HASL	6×6	0.4343	0.4932	0.6726
EML4	3×3	—	—	0.6696
	6×6	—	—	0.6694
	12×12	—	—	0.6693
QUAD4	3×3	—	—	0.6708
	6×6	—	—	0.6696
	12×12	—	—	0.6694
QUAD9	6×6	—	—	0.6694
	12×12	—	—	0.6693
<i>FSDT</i>	—	0.4337	0.4921	0.6693

at point $x_1 = a/12, x_2 = a/12$ are plotted for several values of the side-to-thickness ratio a/h .

SSL: Double sinusoidally distributed load

In this case, the following normalization of displacement is used in the presentation of results, instead of Eq. (61):

$$\bar{u}_3 = \frac{\pi^4 Q h^3}{12 q_0 a^4} u_3, \quad (62)$$

Table 5: Normalized deflection, u_3 , measured at the center of a simply-supported square laminated $[0/90/90/0]$ plate under UDL.

a/h	mesh	100	20	10
HASL	3×3	0.6884	0.7751	1.0364
	6×6	0.6844	0.7689	1.0253
ANSYS	3×3	0.6894	0.7693	1.0249
	6×6	0.6844	0.7694	1.0250
FSDT	—	0.6833	0.7694	1.0250

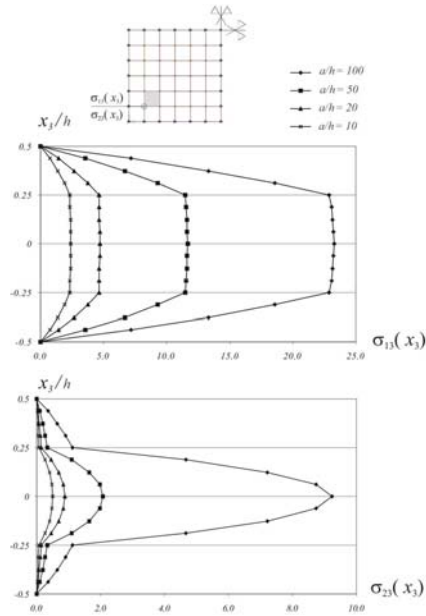


Figure 12: Distribution of shear stresses σ_{13} and σ_{23} at point $(a/12, a/12)$ for the laminate $[0/90/90/0]$ under UDL for different a/h ratios.

where

$$Q = 4G_{12} + \frac{E_1 + E_2(1 + 2\nu_{23})}{1 - \nu_{12}\nu_{21}}. \quad (63)$$

Table 6 presents the normalized deflection of the plate center for the present load case. Along with some numerical results available in the literature, the following analytical solutions are reported for comparison purposes: FSDT; *Higher order* plate theory by [18]; 3-D elastic theory, provided by [22].

Finally, in Figure 13 the distribution of transversal shear stresses $\sigma_{13}(x_3)$ and $\sigma_{23}(x_3)$ at point $x_1 = a/12, x_2 = a/12$ are plotted for several values of the side-to-thickness ratio a/h .

Table 6: Deflection, u_3 , normalized according to Eq. (62) measured at the center of a simply-supported square laminated [0/90/90/0] plate under SSL.

a/h	mesh	100	50	10
HASL	6×6	1.007	1.024	1.548
EML4	5×5	—	—	1.727
PHSL	4×4	1.0060	1.0306	1.7154
CTMQ20	4×4	1.007	1.031	1.735
	8×8	1.008	1.031	1.729
	16×16	1.008	1.031	1.728
DST	10×10	—	1.067	1.727
REC56-Z0	2×2	0.956	0.993	1.445
REC72-Z0	2×2	0.962	1.006	1.663
FSDT	—	1.006	—	1.537
Higher order	—	1.0034	1.0275	1.6712
3-D	—	1.008	1.031	1.733

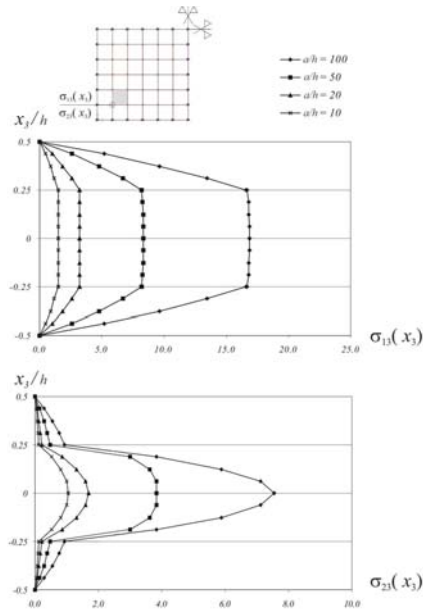


Figure 13: Distribution of shear stresses σ_{13} and σ_{23} at point $(a/12, a/12)$ for the laminate [0/90/90/0] under SSL for different a/h ratios.

It should be noticed, by making reference to the transversal deflection, that the results provided by the HASL element are in good agreement with those of the 3-D solution for all the side-to-thickness ratio. Like in all other cases no shear-locking

phenomena occurs in the thin plate limit.

Acknowledgement

The financial support of both MIUR, the Italian Ministry of Education, University and Research (under Grant Cofin 2003: *Interfacial Damage Failure in Structural Systems: Applications to Civil Engineering and Emerging Research Fields*) and the University of Trento is gratefully acknowledged.

The research project has been partially developed during a research stay of E. Garusi at UCLA with a research grant provided by Prof. S.N. Atluri.

References

1. S. N. Atluri. Recent studies of hybrid and mixed finite element methods in mechanics. In S. N. Atluri and et. al. , editors, *Hybrid and Mixed Finite Element Methods*, J. Wiley & Sons, pages 51–72, 1983.
2. F. Auricchio and E. Sacco. A mixed-enhanced finite-element for the analysis of laminated composite plates. *International Journal for Numerical Methods in Engineering*, 69:1481–1504, 1999.
3. F. Auricchio and E. Sacco. Refined first-order shear deformation theory models for composite laminates. *Journal of Applied Mechanics ASME*, 70:381–390, 2003.
4. K. J. Bathe. *Finite element procedures*. Prentice Hall, Englewood Cliffs, NJ, 2nd edition, 1996.
5. P. Bisegna and E. Sacco. A layer-wise laminate theory rationally deduced from the three-dimensional elasticity. *Journal of Applied Mechanics ASME*, 64:538–545, 1997.
6. F. Brezzi and M. Fortin. *Mixed and hybrid finite element methods*. Springer, New York, 1st edition, 1991.
7. A. Cazzani and S. N. Atluri. Four-noded mixed finite elements, using unsymmetric stresses, for linear analysis of membranes. *Computational Mechanics*, 11:229–251, 1993.
8. S. Cen, Y. Long, and Z. Yao. A new hybrid-enhanced displacement-based element for the analysis of laminated composite plates. *Computers & Structures*, 80:819–833, 2002.
9. V. E. Chepiga. Refined theory of multilayered shells. *Soviet Applied Mechanics*, 12:1127–1130, 1976. English translation from *Prikladnaia mekhanika*, vol. 12, pp. 45–49.
10. P. Cicala. Consistent approximations in shell theory. *Journal of the Engineering Mechanics Division ASCE*, 88:45–74, 1962.

11. M. Di Sciuva. An improved shear deformation theory for moderately thick multi-layered anisotropic shells and plates. *Journal of Applied Mechanics*, 54:589–596, 1987.
12. E. Garusi, A. Cazzani, and A. Tralli. An unsymmetric stress formulation for Reissner-Mindlin plates: a simple and locking-free hybrid rectangular element. *International Journal of Computational Engineering Science*, 2004. In print.
13. E. Garusi and A. Tralli. A hybrid stress-assumed transition element for solid-to-beam and plate-to-beam connections. *Computers & Structures*, 80:105–115, 2002.
14. P. Gaudenzi, A. Mannini, and R. Carbonaro. Multi-layer higher order finite elements for the analysis of free-edge stresses in composite laminates. *International Journal for Numerical Methods in Engineering*, 41:851–873, 1998.
15. T. J. R. Hughes. *The finite element method—Linear static and dynamic finite element analysis*. Prentice Hall, Englewood Cliffs, NJ, 1st edition, 1987.
16. P. Lardeur and J. L. Batoz. Composite plate analysis using a new discrete shear triangular finite element. *International Journal for Numerical Methods in Engineering*, 27:343–359, 1989.
17. W. Liou and C. T. Sun. A three-dimensional hybrid stress isoparametric element for the analysis of laminated composite plates. *Computers & Structures*, 25:241–249, 1987.
18. K. H. Lo, R. M. Christensen, and E. M. Wu. A higher-order theory of plate deformation: Part 2, laminated plates. *Journal of Applied Mechanics ASME*, 44:669–676, 1977.
19. S. T. Mau, P. Tong, and T. H. H. Pian. Finite element solutions for laminated plates. *Journal of Composite Materials*, 6:304–311, 1972.
20. R. D. Mindlin. Influence of rotatory inertia and shear on flexural motions of isotropic elastic plates. *Journal of Applied Mechanics ASME*, 18:31–38, 1951.
21. A. K. Noor and W. S. Burton. Assessment of computational models for multilayered anisotropic plates. *Composite Structures*, 14:233–265, 1990.
22. N. J. Pagano. Exact solutions for rectangular bidirectional composites and sandwich plates. *Journal of Composite Materials*, 4:20–34, 1970.
23. N. J. Pagano and S. J. Hatfield. Elastic behavior of multilayered bidirectional composites. *AIAA Journal*, 10:931–933, 1972.

24. P. F. Pai. A new look at shear correction factors and warping functions of anisotropic laminates. *International Journal of Solids and Structures*, 32:2295–2313, 1995.
25. B. N. Pandya and T. Kant. Flexure analysis of laminated composites using refined higher-order C0 plate bending elements. *Computer Methods in Applied Mechanics and Engineering*, 66:173–198, 1988.
26. V. V. Poniatovskii. Theory for plates of medium thickness. *PMM*, 26:478–486, 1962. English translation from *Prikladnaia Matematika i Mekhanika*, vol. 26, pp. 335–341.
27. E. F. Punch and S. N. Atluri. Applications of isoparametric three-dimensional hybrid-stress finite elements with least-order stress fields. *Computers & Structures*, 19:409–430, 1984a.
28. E. F. Punch and S. N. Atluri. Least-order, stable, invariant isoparametric hybrid finite elements for linear continua and finitely deformed plates. In *Proceedings of the 25th AIAA/ASME/ASCE Structures, Structural Dynamics and Materials Conference*, Palm Springs, CA, pages 190–202, 1984b.
29. Y. Qi and N. F. Knight. A refined first-order shear-deformation theory and its justification by plane-strain bending problem of laminated plates. *International Journal of Solids and Structures*, 33:49–64, 1996.
30. J. N. Reddy. A simple higher-order theory for laminated composite plates. *Journal of Applied Mechanics ASME*, 51:745–752, 1984.
31. J. N. Reddy. A generalization of two-dimensional theories of laminated composite plates. *Communications in Applied Numerical Methods*, 3:173–180, 1987.
32. J. N. Reddy. *Mechanics of laminated composite plates and shells—Theory and analysis*. CRC Press, Boca Raton, FL, 2nd edition, 2004.
33. E. Reissner. The effect of transverse shear deformation on the bending of elastic plates. *Journal of Applied Mechanics ASME*, 12:69–77, 1945.
34. D. H. Robbins and J. N. Reddy. Modeling of thick composites using a layer-wise laminate theory. *International Journal for Numerical Methods in Engineering*, 36:655–677, 1993.
35. R. Rolfes and K. Rohwer. Improved transverse shear stresses in composite finite elements based on first order shear deformation theory. *International Journal for Numerical Methods in Engineering*, 40:51–60, 1997.
36. R. Rolfes, K. Rohwer, and M. Ballerstaedt. Efficient linear transverse normal stress analysis of layered composite plates. *Computers & Structures*, 68:643–

652, 1998.

37. E. A. Sadek. Some serendipity finite elements for the analysis of laminated plates. *Computers & Structures*, 69:37–51, 1998.
38. M. Savoia, F. Laudiero, and A. Tralli. A refined theory for laminated beams: Part I—a new high-order approach. *Meccanica*, 28:39–51, 1993.
39. M. Savoia, F. Laudiero, and A. Tralli. A two-dimensional theory for the analysis of laminated plates. *Computational Mechanics*, 14:38–51, 1994.
40. G. Singh, K. K. Raju, and G. V. Rao. A new lock-free, material finite element for flexure of moderately thick rectangular composite plates. *Computers & Structures*, 69:609–623, 1998.
41. R. L. Spilker. Hybrid-stress eight-node element for thin and thick multi-layered laminated plates. *International Journal for Numerical Methods in Engineering*, 18:801–828, 1982.
42. R. L. Spilker and N. I. Munir. A hybrid-stress quadratic serendipity displacement Mindlin plate bending element. *Computers & Structures*, 12:11–21, 1980.
43. R. L. Spilker, O. Orringer, and E. A. Witmer. Use of the hybrid-stress finite element model for the static and dynamic analysis of composite plates and shell. *Technical Report ASRL TR 181–2*, MIT, 1976.
44. S. Vlachoutsis. Shear correction factors for plates and shells. *International Journal for Numerical Methods in Engineering*, 33:153–1552, 1992.
45. K. Washizu. *Variational methods in elasticity and plasticity*. Pergamon Press, Oxford, 3rd edition, 1982.
46. J. M. Whitney. Shear correction factors for orthotropic laminates under static load. *Journal of Applied Mechanics ASME*, 40:302–304, 1973.
47. J. M. Whitney and N. J. Pagano. Shear deformation in heterogeneous anisotropic plates. *Journal of Applied Mechanics ASME*, 37:1031–1036, 1970.
48. W.-M. Xue and S. N. Atluri. Existence and stability, and discrete B and rank conditions, for general mixed-hybrid finite elements in elasticity. In R. L. Spilker, editor, *Hybrid and Mixed Finite Element Methods*, AMD, volume 73, pages 91–112, 1985.
49. P. C. Yang, C. H. Norris, and Y. Stavsky. Elastic wave propagation in heterogeneous plates. *International Journal of Solids and Structures*, 2:665–684, 1966.

50. T. Yoda and S. N. Atluri. Post-buckling analysis of stiffened laminated composite panels, using a higher-order shear deformation theory. *Computational Mechanics*, 9:390–404, 1992.
51. Y-K. Yong and Y. Cho. Higher-order, partial hybrid stress, finite element formulation for laminated plate and shell analysis. *Computers & Structures*, 57:817–827, 1995.
52. W. Yu, D. H. Hodges, and V. V. Volovoi. Asymptotically accurate 3-D recovery from Reissner-like composite plate finite elements. *Computers & Structures*, 81:439–454, 2003.
53. O. C. Zienkiewicz and R. L. Taylor. *The finite element method*. McGraw-Hill, New York, 4th edition, 1991.

